addenda and errata

Variable-period undulators as synchrotron radiation sources. Erratum

G. K. Shenoy,[a]* J. W. Lewellen,[a] Deming Shu[a] and N. A. Vinokurov[a,b]

[a]Advanced Photon Source, Argonne National Laboratory, Argonne, IL 60439, USA, and [b]Budker Institute of Nuclear Physics, 630090 Novosibirsk, Russian Federation. E-mail: gks@aps.anl.gov

Citations are added to the paper by Shenoy *et al.* [*J. Synchrotron Rad.* (2003). **10**, 205–213].

The authors regret the following unintentional omission of citations which have described earlier the potential for variable-period undulators (Shenoy *et al.*, 2003), and would like to thank Dr Roman Tatchyn for bringing this to our attention: Tatchyn, R. (1989). *Nucl. Instrum. Methods Phys. Res. A*, **275**, 430–434; Tatchyn, R. & Cremer, T. (1990). *IEEE Trans. Magn.* **26**, 3102–3123.

References

Shenoy, G. K., Lewellen, J. W., Shu, D. & Vinokurov, N. A. (2003). *J. Synchrotron Rad.* **10**, 205–213.

Variable-period undulators as synchrotron radiation sources

G. K. Shenoy,[a]* J. W. Lewellen,[a] Deming Shu[a] and N. A. Vinokurov[a,b]

[a]*Advanced Photon Source, Argonne National Laboratory, Argonne, IL 60439, USA, and* [b]*Budker Institute of Nuclear Physics, 630090 Novosibirsk, Russian Federation.*
E-mail: gks@aps.anl.gov

A concept for variable-period undulators for the production of synchrotron radiation from both medium- and high-energy storage rings is described. This concept is based on a staggered array of permeable poles placed in a magnetic solenoid that produces a longitudinal field. The concept permits variations in the short magnetic period of the undulator of as much as 100%. The unique capabilities of such undulators will allow them to be tuned by the variation of the period length and of the solenoid field. The device can be operated at either constant flux or constant power, independent of X-ray energy. It is expected that the new concept will have a major impact on the production and applications of X-rays because of the inherent simplicity and flexibility of the design and the absence of radiation damage. Analyses of the magnetic and mechanical design concepts are presented.

1. Introduction

Permanent-magnet undulators have dominated the synchrotron radiation scene as the most desirable sources over the two decades since their discovery (Halbach, 1981; Brown *et al.*, 1983; Kornyukhin *et al.*, 1983). Such undulators, with magnetic periods ranging from 1.6 cm to many cm, are common to most of the third-generation light sources (Chavanne *et al.*, 1998; Gluskin, 1998; Kitamura, 1988). Recently, there has been a growing interest in the use of permanent-magnet undulators to deliver radiation of up to 80–100 keV (Shastri *et al.*, 1998) at high-energy storage rings (6–8 GeV) and of up to 10–15 keV (Clarke & Scott, 2001) at medium-energy storage rings (2.4–3.0 GeV). However, these energies can only be achieved through a combined use of very high harmonics of radiation, small undulator periods and small undulator gaps. Small gaps and small periods have been incorporated into undulator designs to meet some needs (Rakowsky *et al.*, 2001; Hara *et al.*, 1998; Stefan *et al.*, 1998; Tanabe *et al.*, 1998) and also into superconducting designs (Geisler *et al.*, 2001). These approaches have often been encumbered by either an increase in the total power delivered by the undulator or the limited tunability of the radiation energy. These restrictions have limited the use of small-period undulators to specialized applications at storage-ring-based light sources and free-electron lasers (FELs) [Wulff, 2002 (beamline ID-09 at ESRF employs an in-vacuum undulator with 1.6 cm period and 6 mm gap specifically designed for time-resolved research using 15 keV X-rays); Ho *et al.*, 1991; Varfolomeev *et al.*, 1992].

In the development of IR FEL, the Stanford University group (Huang, Wang, Pantell, Feinstein & Harris, 1994; Huang, Wang, Pantell, Feinstein & Lewellen, 1994; Lewellen *et al.*, 1995) took a novel approach in designing a 1 cm-period undulator. Although their application required a fixed-period undulator to operate at a 2 mm gap, here we use their ideas to design undulators with variable-period capability suitable for light-source applications. The novel undulator consists of a staggered array of permeable poles placed in a longitudinal field generated by a magnetic solenoid. The staggered placement of high-permeability pole pieces to form a periodic structure generates a periodic transverse field along the axis of the device for the production of undulator radiation. The concept has been tested for a fixed-period undulator in a far-infrared FEL (Lewellen *et al.*, 1995).

The new approach discussed here extends the capability of a staggered geometry of poles and allows for the first time a design in which the undulator period can be varied to tune the X-ray energy (Shenoy *et al.*, 2002). The design is attractive for both short- and long-period undulators because of its simplicity and flexibility, but most importantly its performance can exceed that of permanent-magnet undulators. In addition, it is anticipated that the potential new capabilities of the variable-period undulator will enhance the performance of experiments at third-generation synchrotron radiation sources, sources based on energy recovery linacs (ERLs) and FELs.

2. Basic concept

In a planar undulator, the energy harmonics of the radiation are produced when the trajectory of the electron beam along the axis of the undulator is modulated by the spatially periodic transverse magnetic field of the undulator. The X-ray energy of the nth harmonic, E_n, produced along the axis of the undulator is given by

$$E_n \,(\text{KeV}) = 0.95 E^2 \,(\text{GeV})\, n/[\lambda_\mathrm{u} \,(\text{cm})\,(1 + K^2/2)]. \tag{1}$$

In (1), E is the energy of the electrons in a storage ring, ERL or FEL, n is an odd integer, and

$$K = 0.934 \lambda_\mathrm{u} \,(\text{cm})\, B_y(\text{T}), \tag{2}$$

where B_y is the peak value of the periodic magnetic field along **y**.

The period of the permanent-magnet undulator cannot be changed, which limits the energy tunability and many other operational capabilities. In our new concept for an undulator, a variable period is achieved through the use of a staggered array of pole pieces made of a high-permeability material. The rectangular pole pieces have a width d and are separated by a variable-width space, α, as shown in Fig. 1. The set of arrays is placed in a solenoid that produces a uniform longitudinal magnetic field, B_0, and could be a normal-conducting or a superconducting coil. This field is deflected by the pole pieces to generate a periodic transverse field with a period λ_u. Potential high-permeability pole materials are 1010 steel or vanadium permendur.

For a small undulator period, the amplitude of the first field harmonic is approximated (Ho *et al.*, 1991) by the equation
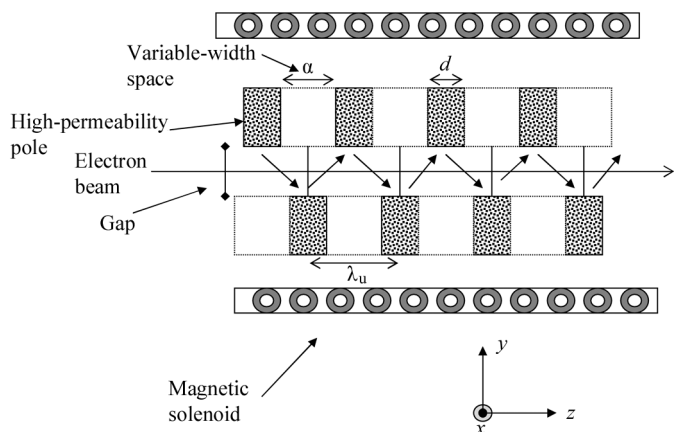
$$B_y = [2B_0 \,/\, \sinh(\pi g/\lambda_\mathrm{u})](\sin \pi f)/(\pi f), \tag{3}$$

where g is the gap and $f = \alpha/\lambda_\mathrm{u}$. It appears from (3) that either increasing the solenoid field, B_0, or reducing the width α to zero can increase the value of B_y. However, the saturation magnetization of the high-permeability poles sets the limit on B_y. In order to fully evaluate the problem in selecting both α and B_0, we present the results of a field calculation in §3.
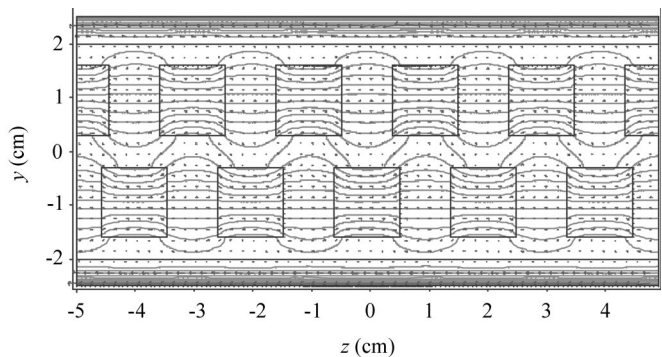
3. Magnetic analysis

A field analysis for a defined geometry of the undulator structure gives considerable insight into the magnetic and mechanical performance of the device (Lewellen *et al.*, 2003). Here we only present a summary of a two-dimensional analysis of the magnetic performance of a variable-period undulator using the *Poisson/SUPERFISH* code (Billen & Young, 2001). It should first be recognized that, as in permanent-magnet hybrid undulators, the maximum value of B_y is determined by the permeability of the pole material. We will use high-permeability 1010 steel in our conservative approach to the design (rather than vanadium permendur, which would provide 15–20% enhancement in field strength). To demonstrate the behavior, two cases have been chosen, *viz.* one with a *minimum* period of $\lambda_u = 1.3$ cm (I) and one with a minimum of $\lambda_u = 1.5$ cm (II). The optimization of $f = \alpha/\lambda_u$ (where the variable-width space $\alpha = \lambda_u - d$) was performed to arrive at the maximum value of B_y, and the results are given in Table 1. The effective value of K (referred to as K_{eff}) is derived from Fourier decomposition of the B_y field [in (2)] that is produced by the staggered poles of the undulator.

The value of α can be increased, while keeping the gap, G, and the pole width, d, fixed, to realize the magnetic period increase within a

Table 1
Optimized values of f and pole width from the Poisson analysis for two cases, and the effective value of K (K_{eff}).

The maximum value of the period is twice the minimum given in the table.

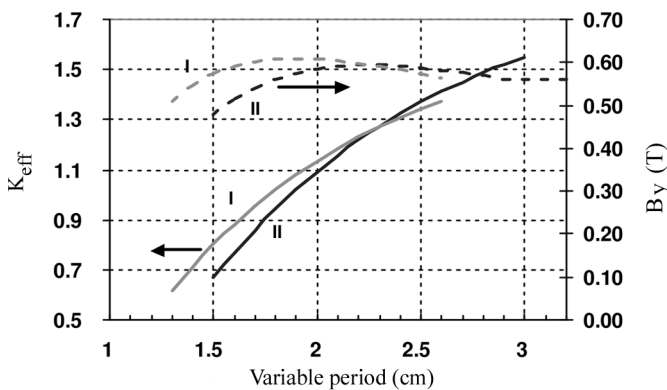|	Minimum period λ_u (cm)	Gap G (cm)	Optimized $f = \alpha/\lambda_u$	Variable-width space α (cm)	Pole width d (cm)	K_{eff}
I	1.3	0.5	0.385	0.53–1.83	0.77	0.62
II	1.5	0.6	0.436	0.37–1.87	1.13	0.67

single device. The value of α given in Table 1 corresponds to the *minimum* value of the periods. A Poisson analysis of the magnetic performance with increasing period shows that the device behaves as an undulator (as opposed to a wiggler) even when the period is twice the minimum period. Note that the undulator length ($L = N\lambda_u$) increases with magnetic-period length, since the number of variable-length periods (N) remains the same within a single undulator. The uniform-field region of the magnetic solenoid is made long enough to take this variability into account. Fig. 2 shows the magnetic-field profile for undulator II. The field lines responsible for the undulator behavior of the staggered-array configuration ride on a longitudinal field, as shown in Fig. 2. The consequences of this longitudinal field are important in the design of the insertion section of the storage ring, as discussed in §5.

In Fig. 3, the variation of K_{eff} as a function of period length is shown for devices I and II. The values of the higher harmonic coefficients of K (K_3 and K_5) were found to be between one and three orders of magnitude smaller than K_{eff} depending on the length of the period. The tunability of the harmonics of the radiation from these devices, based on the variable period, can be calculated for various electron energies using (1).

The value of K_{eff} for any value of the magnetic period, λ_u, in a device (without changing d, G or B_0) is dependent on both λ_u and B_y (see Fig. 3). Also, the values of K_{eff} are generally small, and hence the first two odd harmonics of radiation will be the most intense. Therefore, these devices will produce smaller values for the total radiation power.

For each value of the variable-undulator period, the value of B_0 can be changed to derive additional changes in the value of K_{eff}, thus adding additional tunability of energy harmonics at each value of the magnetic period. In many respects, changing B_0 is equivalent to varying K_{eff} by changing the gap in permanent-magnet undulators.

Figure 1
The basic concept for a variable-period undulator. The spaces with width α permit period variation along the z axis, and the blocks of high-permeability material (1010 steel or vanadium permendur) have a fixed width d. The periodic transverse undulator field is derived by the staggered arrays from the longitudinal field, B_0, produced by the electromagnetic (or a superconducting) solenoid.

Figure 2
The magnetic field lines responsible for the undulator field ride over a constant longitudinal field throughout the device. The illustration is for undulator II (Table 1) for a period of 2.0 cm.

Figure 3
The values of K_{eff} as a function of increasing period length for the two undulators in Table 1. The dashed lines give the value of B_y as the period is increased without changing the value of B_0 (1.3 T).

However, in a given permanent-magnet device, because of its fixed period, the gap variation is the only path to harmonic tunability. In Fig. 4, the variation in K_{eff} for a variable-period undulator ($\lambda_u = 3.3$ cm, $f = 0.5$ and $G = 1.15$ cm) achieved by changing B_0 is shown for (a) 1010 steel and (b) vanadium peremendur poles. The highest value saturates at $K_{eff} \simeq 1.5$. In hybrid-type permanent-magnet undulators, such a variation is achieved only through changes in G, and the resulting value of K_{eff} could be larger by nearly a factor of two at small gaps.

4. New capabilities and advantages of the variable-period undulator

Below we discuss the new capabilities of the variable-period undulator design and point out its advantages over the traditional permanent-magnet undulator.
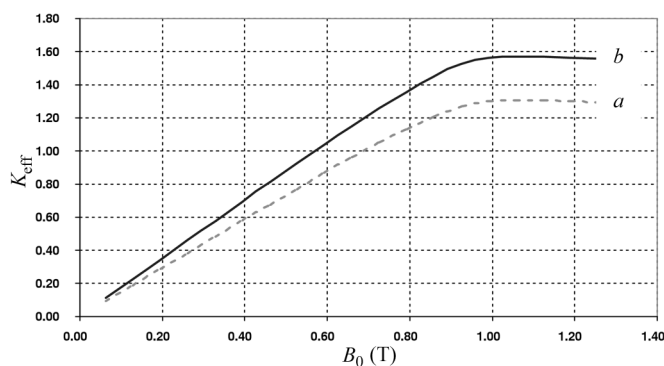
4.1. Variable-period undulator parameters

The design and operational parameters for a variable-period undulator span a broad space defined by the length of the period, the width of the pole pieces, the gap and the solenoid field (λ_u, d, G, B_0). This rich space should be explored during the design in order to meet the specific needs of experiments and the storage-ring parameters. Each of the parameters λ_u, d, G and B_0 will influence both the performance and the tunability, although only the width of the pole pieces cannot be altered during the operation of a device. In contrast, permanent-magnet undulators only have one variable available in the operational phase, *i.e.* the gap value. We have noted above that the changes in λ_u and B_0 are two key elements in achieving a broad variation in K_{eff}. The gap variation can also be incorporated into the design, as is routinely done in hybrid undulators. However, a gap variation may not be necessary in most designs, since its effect on B_y can effectively be mimicked by the variation in B_0.

4.2. Design performance

The design performance of the variable-period undulators is demonstrated by choosing two sets of electron-orbit parameters representative of high-energy (6–8 GeV) and medium-energy (2.4–3 GeV) storage rings. The selected parameters for the storage ring and the undulators are given in Table 2.

As can be seen from Table 1, the selected undulators will require a small gap operation, and hence, in order to avoid small life times for the stored electron beam, it is preferable to operate the storage ring with a 'top-up' injection. This process has been successfully imple-

Table 2
Electron-beam properties used in the calculations to demonstrate the performance through period variation within a single undulator.

Properties	Medium energy†	High energy‡
Energy (GeV)	3.0	7.0
Current (mA)	300	100
Beam size, σ_x (µm)	91.4	254
Beam divergence, σ_x' (µrad)	25.7	15.6
Beam size, σ_y (µm)	7.0	12
Beam divergence, σ_x' (µrad)	2.8	3.0
Electron energy spread (10^{-3})	1.0	1.0
Minimum undulator period (cm)§	1.3	1.5
Number of undulator periods	80	70
Period increase factor	2.0	2.0
Approximate solenoid length (m)	2.2	2.2
Maximum solenoid field (T)	1.3	1.3

† Taken from DIAMOND design. ‡ Current APS operational parameters. § See Table 1 for details.

mented at the Advanced Photon Source (APS) and the Swiss Light Source (SLS) and is being seriously considered by new facilities under design and construction. The values of X-ray beam brilliance, power and power density for various devices were calculated with *XOP* 2.0 (Dejus & Sanchez del Rio, 1996, Sanchez del Rio & Dejus, 1997). Figs. 5–8 demonstrate the design performance of undulator I

Figure 5
The variation in the value of K_{eff} and the energy of the first harmonic as a function of the changing period of undulator I (defined in Table 1) operating on a 3 GeV storage ring (see Table 2).

Figure 6
The values of the brilliance of radiation as a function of the energy of the first and third harmonics delivered by undulator I (defined in Table 1) operating on a 3 GeV storage ring (see Table 2). The performance of undulator I is compared with that of U24, a 2.4 cm-period hybrid permanent-magnet undulator, proposed for DIAMOND.

Figure 4
The values of K_{eff} as a function of B_0 for a variable-period undulator at a period of 3.3 cm. The pole pieces are made of (a) 1010 steel and (b) vanadium permendur.
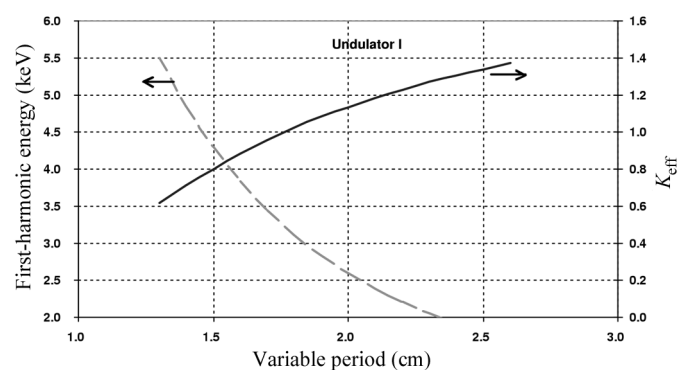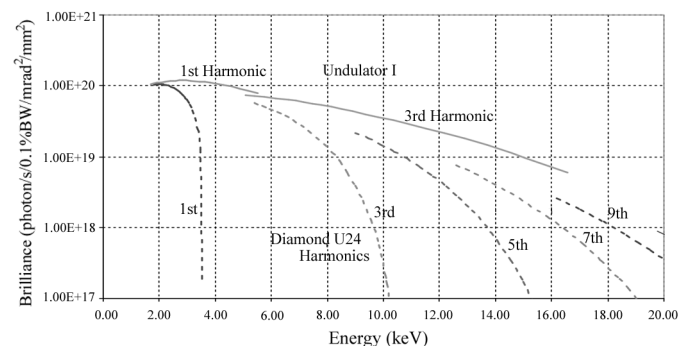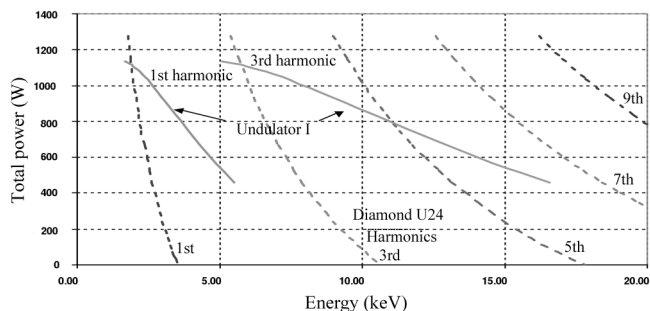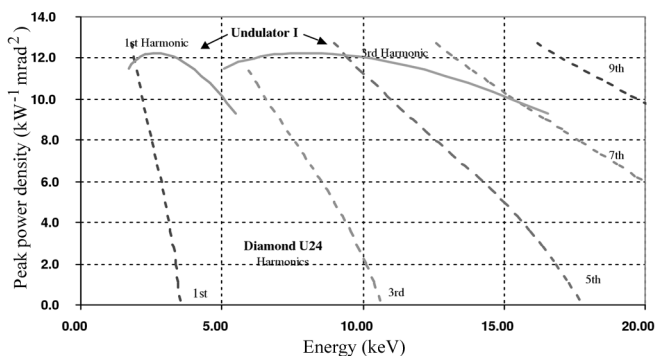
operating on a medium-energy storage ring with the operational parameters given in Table 2. Figs. 9–12 provide the same information for undulator II operating on a high-energy storage ring defined in Table 2. The general performance of these devices is superior to that of any permanent-magnet undulator covering similar X-ray energy ranges on the selected storage rings.
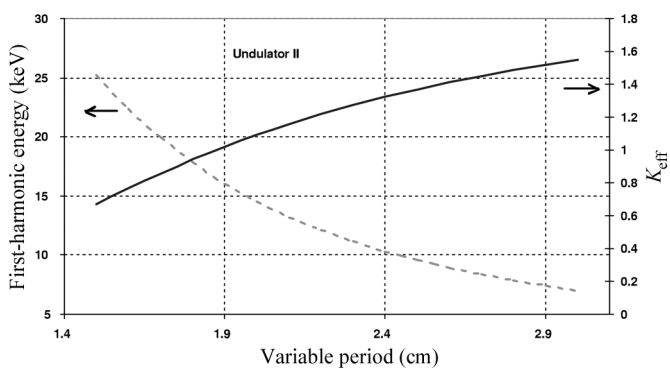
The most notable points from Figs. 5–12 are the following:

(*a*) The values of K_{eff} are smaller by nearly a factor of two for the variable-period undulators compared with hybrid permanent-magnet undulators (*e.g.* Undulator A, currently used at the APS).

(*b*) The brilliance of the radiation from the variable-period undulators is equal to or better than that delivered by comparable permanent-magnet undulators (*e.g.* Undulator A), especially at

Figure 7
The values of total power at various energies of the first and third harmonics delivered by undulator I (defined in Table 1) operating on a 3 GeV storage ring (see Table 2). The performance of undulator I is compared with that of U24, a 2.4 cm-period hybrid permanent-magnet undulator.

Figure 10
The values of the brilliance of radiation as a function of the energy of the first and third harmonics delivered by undulator II (defined in Table 1) operating on a 7 GeV storage ring (see Table 2). The performance of undulator II is compared with that of the APS Undulator A, a 3.3 cm-period hybrid permanent-magnet undulator at the APS.
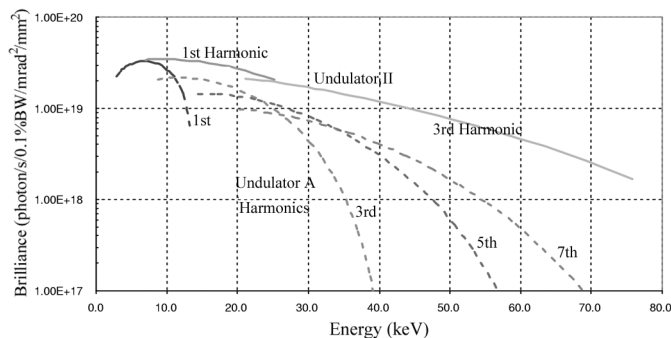

Figure 8
The values of peak power density at various energies of the first and third harmonics delivered by undulator I (defined in Table 1) operating on a 3 GeV storage ring (see Table 2). The performance of undulator I is compared with that of U24, a 2.4 cm-period hybrid permanent-magnet undulator.
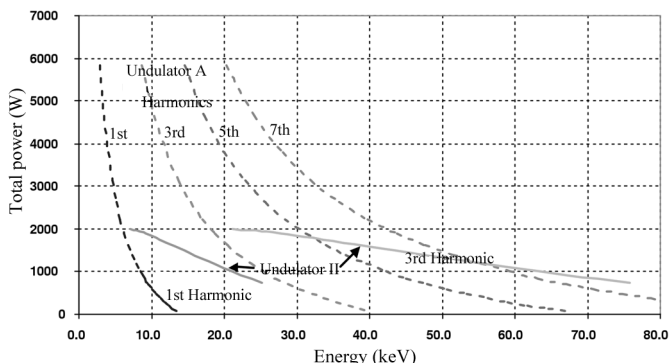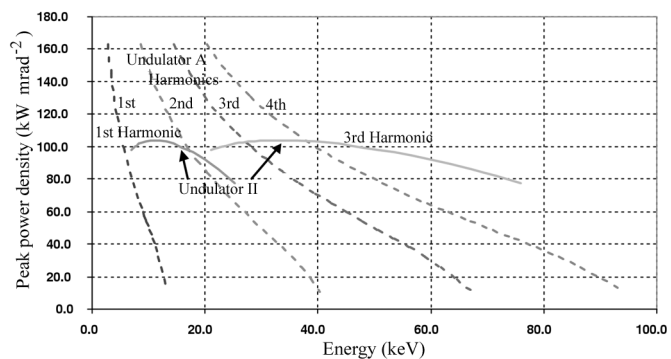

Figure 11
The values of the total power at various energies of the first and third harmonics delivered by undulator II (defined in Table 1) operating on a 7 GeV storage ring (see Table 2). The performance of undulator II is compared with that of Undulator A, a 3.3 cm-period hybrid permanent-magnet undulator at the APS.

Figure 9
The variation in the value of K_{eff} and the energy of the first harmonic as a function of the changing period of undulator II (defined in Table 1) operating on a 7 GeV storage ring (see Table 2).

Figure 12
The values of peak power density at various energies of the first and third harmonics delivered by undulator II (defined in Table 1) operating on a 7 GeV storage ring (see Table 2). The performance of undulator II is compared with that of Undulator A, a 3.3 cm-period hybrid permanent-magnet undulator at the APS.

higher X-ray energies, at both medium- and high-energy storage rings.

(*c*) The new undulators cover a broad tunability range from the first two odd harmonics.

(*d*) The total power from the variable-period undulators is nearly a factor of two lower than that from permanent-magnet undulators, while the power density is comparable, as expected.

4.3. Constant-*K* operation

The variable-period undulator can operate in the unique mode in which the value of K_{eff} is kept fixed. This mode produces a constant photon flux (or brilliance for high-energy X-rays), which is delivered from the device to the first optics and which could be very useful for special experiments. A constant K_{eff} is achieved by reducing the value of B_0 (so that B_y decreases) as λ_u is increased [see (2)]. We have demonstrated this mode of operation for undulator II (Table 1) in Fig. 13.

The constant values of brilliance for the first and the third harmonics when the undulator period is changed from its minimum value to double that value are shown by the lines *AC*. The tunability gap between the first and the third harmonic can be bridged, if desired, by varying the solenoid field (B_0) in order to change B_y at a fixed value of the period. In this demonstration we have chosen to vary B_0 after fixing the period at 2.5 cm. This case is illustrated by the curves *BD*, and the resulting values of various parameters are given in the table as an inset in Fig. 13. The value of B_0 can be varied for any permissible value of the undulator period, thus generating a family of tunability curves of the type *BC*.
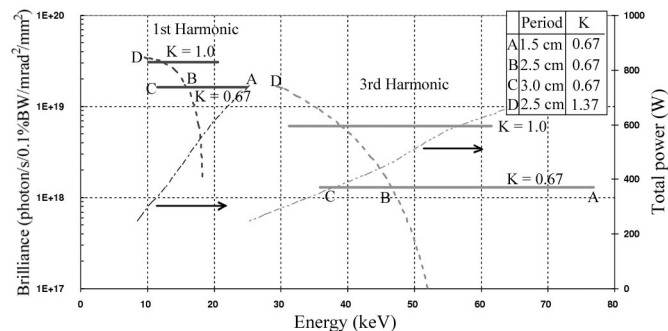
The total power from an undulator with N periods can be expressed as

$$P(W) = 7.64\,NI\,(A)\,K_{eff}^2(1 + K_{eff}^2/2)\,E_n\,(keV)/n, \qquad (4)$$

where I is the stored current in amperes and E_n is the energy of the nth harmonic.

When K_{eff} is a constant, P will be linearly proportional to the X-ray energy, as shown in Fig. 13.

In this example we have demonstrated the flexibility provided by the variable-period undulator in tailoring X-ray beams of constant flux (or brilliance).

4.4. Constant-power operation

Recently, storage rings have been operated in top-up mode, in which the stored current is kept constant (*e.g.* APS, SLS). This mode provides the ability to deliver constant power from an undulator to the first optics at a specific X-ray energy, thus enhancing the X-ray beam stability in performing the experiment. However, if the experiment requires a change in energy, the gap of the permanent-magnet undulator has to be altered, which changes the power load on the first optics. With the flexibility of operation in a variable-period undulator, one can overcome this weakness and maintain constant total power at all X-ray energies by adjusting B_y (or B_0) at each value of the undulator period. It can be shown that the condition for delivering constant power is that $\lambda_u B_y^2$ is a constant. To demonstrate this capability, we will consider a variable-period undulator with a minimum period of 2.0 cm and a gap of 0.7 cm, optimized for $f = 0.43$. The values of B_y corresponding to different periods that will generate a constant power when operated on a high-energy storage ring (see Table 2) are shown in Fig. 14. The resulting values for the first-harmonic energy at different periods are also shown in the graph. The value of the total power from the undulator at all tunable energies is 1.25 kW.
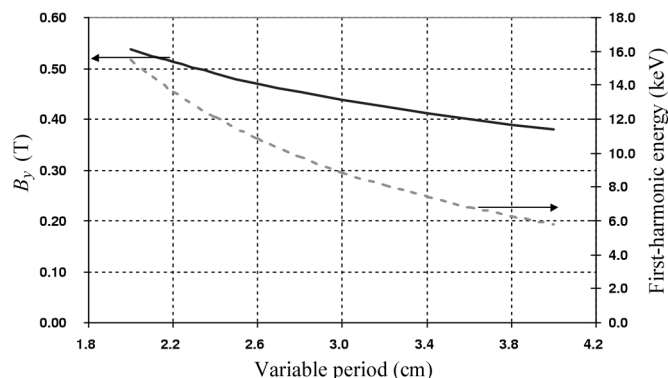
4.5. Modulating or switching between X-ray energies

Many experiments require the ability to modulate the X-ray energy of the harmonics over a small energy range (*e.g.* spectroscopy) or switch between two or more fixed energy values (*e.g.* anomalous scattering, multiple-wavelength anomalous dispersion). This ability can easily be achieved by superimposing a programmed variable current on the solenoid generating B_0, which is phase locked to the experimental equipment (*e.g.* stepping motors, piezodrivers).

The equivalent of a tapered undulator configuration, which is currently used to increase the energy width of a harmonic, can also be realized by superposing a ramped field of appropriate amplitude over B_0.

4.6. Very long undulators for FEL applications

An undulator based on a staggered pole configuration with a fixed period has been successfully used to produce IR radiation from an FEL (Lewellen *et al.*, 1995). With this success, it is natural to think of the undulator's applicability for UV and X-ray FELs, which require long undulator lengths. In principle, the new devices can be assem-

Figure 13
The constant-K_{eff} operational mode results in nearly constant brilliance values for undulator II, as shown by lines *AC* for the first and the third harmonics (the period is changed from 1.5 cm to 3.0 cm, see inset). The dashed curves *BD* were obtained by varying the solenoid field after the period was fixed at 2.5 cm. The total power is linearly proportional to the X-ray energy when it is kept fixed, as shown by thin dashed lines.

Figure 14
A graph demonstrating the constant-power mode of operation of a variable-period undulator with a minimum 2.0 cm period operating on the high-energy storage ring (Table 2). The values of B_y required to maintain constant power at all X-ray energies is shown as a function of the variable period.

bled over very long lengths, making them suitable for self-amplified spontaneous emission (SASE) FEL applications with the added bonus of both variable-K capability (through B_0 change) and variable-period-length capability. While the use of these undulators will add tunability to FEL radiation, there are many challenges in realizing such a potential. For example, the effect on FEL gain when the length of the drift spaces between the undulator segments changes (resulting from the alteration in undulator period length) requires further study (Gippner, 2001).

4.7. New and unique radiation properties

The simplicity of the device design and construction will lead to new geometrical arrangements and shapes of staggered poles and to solenoid fields that are capable of producing synchrotron radiation with new properties to meet both unanticipated needs of research and established needs. A helical undulator geometry is an obvious example.

4.8. Optimizing power loads on front ends and optics

One important consideration for experimenters is to ensure that most of the total radiation power (P_T) produced by the undulator arises from the harmonic (P_n) that is used. The flexibility in varying the period and the solenoid field, B_0, provides a unique opportunity to optimize the ratio P_n/P_T. For example, in the illustration discussed in §4.4, 56% of the power is in the first harmonic and 27% is in the third. A variable-period undulator, intrinsically being a small K_{eff} device as opposed to a permanent-magnet device, truly behaves like an undulator by providing most of the power to the useful part of the spectrum.

4.9. Operational environment

The staggered-pole arrays in a variable-period undulator can be placed in ambient pressure surrounding the electron-beam vacuum chamber in a straight section of the storage ring or an ERL. In order to achieve smaller undulator gaps (e.g. 4 mm), the staggered arrays may be placed inside the accelerator vacuum chamber in a way similar to that used in the in-vacuum undulators currently in use, since all components are UHV-compatible metals.

4.10. Magnetic solenoid

The solenoid could be either a normal-conducting or a super-conducting coil. These solenoids are relatively simple to build and are capable of producing a highly uniform field over the length of the undulator arrays without any shimming. The solenoids are commercially produced to the required specifications.

4.11. Absence of radiation degradation

The magnetic material in permanent-magnet undulators is susceptible to degradation, primarily from photoneutrons produced from bremsstrahlung, electron-beam dumps and intense X-ray FEL pulses. This is particularly serious at small gaps and in-vacuum configurations. The materials in the new undulator are generally free from such damage issues and hence are suitable for small-gap operational needs in storage rings, ERLs and FELs.

## 5. Undulator magnetic design considerations and meeting the accelerator requirements

In general, the installation of an undulator in a storage-ring lattice degrades the overall performance of the lattice unless special care is taken in the magnetic design of the undulator. For each storage ring it

is hence essential to set limits on the undulator magnetic-field quality, which is defined by various field integrals such that the undulator is transparent to the electron trajectory. As for any insertion device, the manufacturing errors should be reduced such that the measured field integrals meet the specifications. Also, the undulator will contribute to the trajectory kicks as the electron enters and leaves the device. In addition, unlike conventional undulators, the variable-period undulator has a longitudinal solenoid field, which will produce both focusing of the electron beam and transverse coupling. In the following, we provide a brief summary of the aspects that are considered in the magnetic design.

5.1. End correctors

For an undulator with finite length, it is important to design the end configurations of the magnetic structure to effectively eliminate the trajectory kick for any operational configuration of the undulator, such as the value of B_0 or the period. Masuda et al. (2001) have carried out a detailed analysis that has focused on such refinements in a fixed-period staggered-array undulator. The refinements suggested here to resolve these issues in the present concept for the device include the addition of 'shielding' blocks at each end of the device, perhaps with slightly different gaps from those for the main staggered arrays. An improved uniformity in the magnetic-field profile throughout the solenoid can be achieved by adding end-cap correctors to the solenoid, and the transverse coupling is compensated using guard coils (see §5.3). The general layout of the device is shown in Fig. 15(a). The variation of the undulator field along the length of the 2.4 m-long device with the above refinements is shown in Fig. 15(b), along with the trajectory of a 7 GeV electron passing through this undulator with a 6 mm gap. The field profile and the trajectory are shown in more detail over six periods in the middle of Fig. 15(b).

While this modeling requires further refinement, the results are already satisfactory. All the trajectory errors are well within acceptable tolerances for the APS, as discussed below.
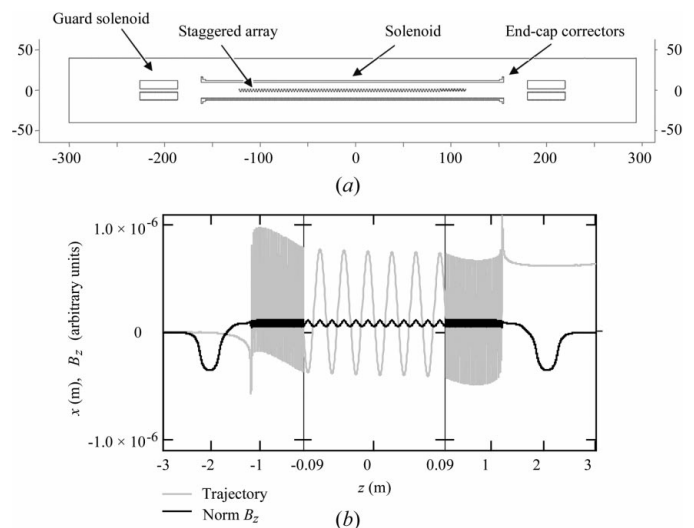
Figure 15
(a) The general layout of the variable-period undulator, showing the staggered array, with end correctors placed in a solenoid with end caps, and guard coils to compensate for transverse coupling (see §5.3). (b) The on-axis magnetic field in the zy plane of undulator II, with a period of 3.0 cm, $K = 1.0$, $B_0 = 0.75$ T, and $G = 6$ mm. The 7 GeV electron trajectory in the zx plane of a 80 period-long undulator, with the inclusion of the end pole configuration, solenoid end caps and guard coils, is shown. The details are shown for six periods in the middle.

5.2. Field integrals

This analysis has been extended to determine the values of various field integrals and to compare them with the acceptable tolerances that will allow us to treat the undulator as transparent to the motion of the electrons in a third-generation storage ring. Since no device has been built, the mechanical-design tolerances were assessed from the Poisson analysis by introducing pole-placement errors in both the y and the z directions. The first two field integrals for the variable-period undulators are well within the acceptable specifications for a third-generation storage ring like the APS (Chae & Decker, 1996). For example, for the APS lattice, the first- and second-field integrals should be less than 50 Gauss cm and 105 Gauss cm^2, respectively. The magnetic analysis for 1.5 cm- and 3.0 cm-period devices showed that, even with r.m.s. pole-placement errors of as large as 100 μm along both z and y, the tolerance budgets can be met. This result is not surprising, since each pole piece in the new device influences the field of a complete undulator period, and hence the effect of the placement errors is relatively small on the net trajectory through the device. It is also comforting to note the earlier (Chae & Decker, 1996) observation that, if the first two field integrals are within the specified budget for a storage ring, the requirements on the multipole tolerances are also satisfied. The details of these requirements should be assessed for each of the storage rings where this new device will be used. While the above analysis shows a weak influence of pole-placement error on the electron-beam trajectory, the pole-placement error has a more serious effect on the radiation properties, as discussed in §5.4.

5.3. Transverse coupling

As mentioned earlier, a new topic in the magnetic design of variable-period undulator is the influence of the longitudinal field on the electron trajectory. This field will cause transverse coupling. A simple analytical estimate of coupling-compensation conditions is given in Appendix A. It is shown that, in the linear approximation, the coupling-compensation conditions are set by the following requirements for the behavior of the magnetic field B in the undulator: (i) a 'two-dimensional' magnetic field $\mathbf{B}(y, z)$, $B_x = 0$; (ii) $\int_{-\infty}^{\infty} B_z(0, z) \, dz = 0$; (iii) $\int_{-\infty}^{\infty} \int_{-\infty}^{z} B_z(0, z_1) \, dz_1 dz = 0$.

The simplest way to achieve these conditions is to add two identical guard coils with rectangular cross sections at the ends of the undulator solenoid, the sum of the ampere-turns in all the solenoids being zero. If all the solenoids are 'flat' ($B_x = 0$), their edges do not transform the horizontal beam size to the vertical angle spread, and the vertical projection emittance in an undulator does not increase. Therefore betatron coupling does not change radiation properties in this scheme. The choice of compensation scheme is specific to the storage-ring lattice and there are other ways to accomplish the compensation of transverse beam rotation. This is also the case in single-pass devices such as ERLs and FELs, which are discussed elsewhere (Lewellen et al., 2003).

5.4. Phase errors

The spectral performance of an undulator is mostly determined by the phase error, which is governed by the pole-to-pole slippage between electron and radiation phases.

We have performed preliminary two-dimensional modeling of the device to assess the dependence of phase errors on the pole-placement errors along y and z. With r.m.s. pole-placement errors of 25 μm in both the y and z dimensions introduced onto every pole piece, the r.m.s. phase error was found to be about 4° and 6° for undulators with 1.5 cm and 3.0 cm period, respectively. Fortunately, a variable-period undulator operates at low K_{eff} values and uses only the first two odd

harmonics, as discussed in §4. The analytical model predicts that the relative intensity of the nth harmonic peak is determined by $\exp[-(n\varphi)^2]$, where φ is the phase error (Walker, 1993; Dejus et al., 2002). Thus we can accept phase errors larger than those required in permanent-magnet undulators, which use higher harmonics. For short periods and low K values, there are no problems with phase errors and therefore with mechanical tolerances. More details will be reported elsewhere (Lewellen et al., 2003).

6. Mechanical design considerations

The mechanical tolerances to achieve acceptable values for field integrals and phase errors have been addressed in §5. It is clear that in a variable-period undulator the largest errors will arise from period-to-period length variations, and therefore the magnet-phase error is the correct parameter to be reduced in the design phase. The mechanical design of the undulator should hence focus on minimizing the period-length variation along the length of the device and on maintaining excellent reproducibility of periods while tuning.

It is also important to consider various magnetic forces acting within the device when developing the mechanical design. From the magnetic analysis it is determined that the forces between the upper and lower staggered arrays of poles in the y direction are almost a factor of two weaker than those in similar permanent-magnet undulator structures. This trend is expected, since the staggered poles do not line up directly above each other. The forces between poles in the z direction would generally cancel for a perfectly symmetric configuration. Fortunately, the magnetic analysis has shown that even if the deviations of the order of a fraction of a millimeter occur, the resulting forces are of minimal consequence in the design.

All the above considerations have set a global tolerance in the mechanical design of about ±25 μm in the placement of poles in the z and y directions, which results from various operational configurations of the undulator including the variation in its period (Lewellen et al., 2003).

When the undulator period is varied, every pole has to move in unison within the above-specified tolerances over large linear travel distances. In order to achieve this level of superior mechanical performance, we propose to incorporate three motion controls that will assist each other. These concepts are summarized below.

A pantograph provides the primary motion for period variation. This parallel-motion linkage is used to provide motion along one direction over large distances. Such a scheme is shown in Fig. 16(a). While pantographs are easy to build and operate, their ability to provide a motion in unison over the entire structure is limited. They can introduce both cumulative errors and backlash. Hence we have added counter-screw motion actuators that establish a natural lock on the entire device with very high precision, as shown in Fig. 16(b). This counter-screw motion may not be required between every pair of poles, and this requirement will be assessed during the detailed design phase. Finally, to balance uneven forces that may develop during the linear motion, constant restoring-force springs are added to the design.

The complete mechanical design should also include supporting and guiding structures for the variable-period undulator around the vacuum chamber. In addition, the entire assembly must fit inside the solenoid. Various configurations have been considered for such an assembly (Shenoy et al., 2002). One of the options, in which the two arrays are independently mounted on the top and the bottom faces of the vacuum chamber, is presented in Fig. 16(c). Both the pantograph and the counter-screw motions are in the zx plane.

In addition, it is important to ensure that the vacuum chamber remains straight over its length to better than ±100 µm, both after the vacuum bake (Den Hartog *et al.*, 1997) and during the undulator operation under the variable stress that might result from the motion of pole pieces. All these considerations form the basis for the final design (Shu *et al.*, 2003).

Finally, Fig. 17 gives a three-dimensional schematic incorporating the concepts shown in Fig. 16.

Note that the mechanical design presented here can, in principle, be used to vary the period in a permanent-magnet undulator. However, the magnetic considerations do not favor this approach above the solenoid-based undulator concept presented in this paper.

7. Conclusions

It is demonstrated here that the ability to vary the length of the undulator period adds many new capabilities that are beyond those of current undulators operating on third-generation synchrotron radiation sources. A new concept that uses arrays of staggered poles of high-permeability material placed inside a magnetic solenoid is presented, which permits large variations in the undulator period. The paper discusses a detailed magnetic analysis to demonstrate the feasibility of the new device. The mechanical design is critical to the performance of such a device. Concepts for a mechanical design that could meet the required tolerances are presented.

There are many challenges in developing a complete design and a working model for a variable-period undulator. However, there are no fundamental limitations to building and implementing such a device on a third-generation storage ring, on an ERL or on an FEL.

APPENDIX *A*
### Coupling-compensation conditions for a staggered-array undulator

The electron trajectory in a planar staggered-array undulator may be described by the Hamiltonian

$$H = -P_z = -\left\{ p^2 - P_y^2 - \left[P_x - eA(y, z)/c \right]^2 \right\}^{1/2}, \qquad (5)$$

where p is the particle kinetic momentum (which is constant in the magnetic field), $\mathbf{P}$ is the canonic momentum, e is the electron charge, c is the velocity of light and A is the x component of the magnetic vector potential. The latter is chosen so that only this component is non-zero. Moreover, A is zero outside the magnetic system. The paraxial expansion of (5) gives

$$H \simeq P_y^2/2p + \left[P_x - eA(y, z)/c \right]^2/2p + p. \qquad (6)$$

The corresponding trajectory equations are
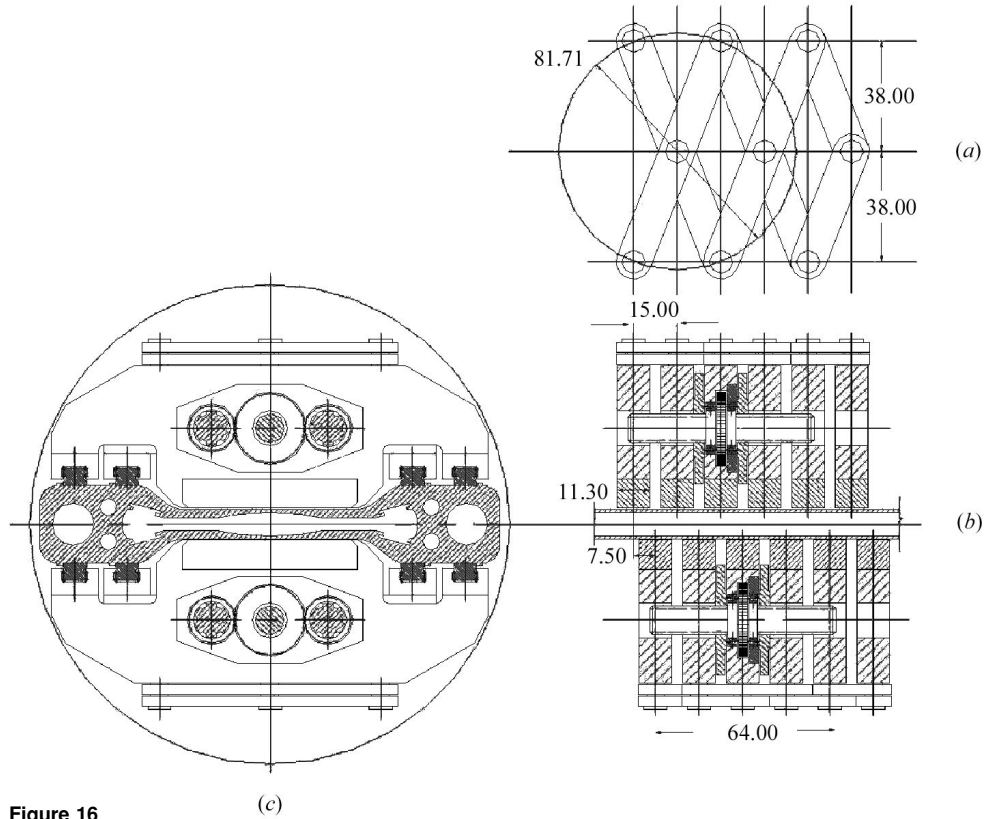
Figure 16
Schematics of the various design components included in providing high-precision linear motion in the variable-period undulator. (*a*) Pantograph motion, (*b*) counter-screw motion and (*c*) supporting and guiding structure around the undulator-vacuum chamber. Dimensions are given in millimetres.
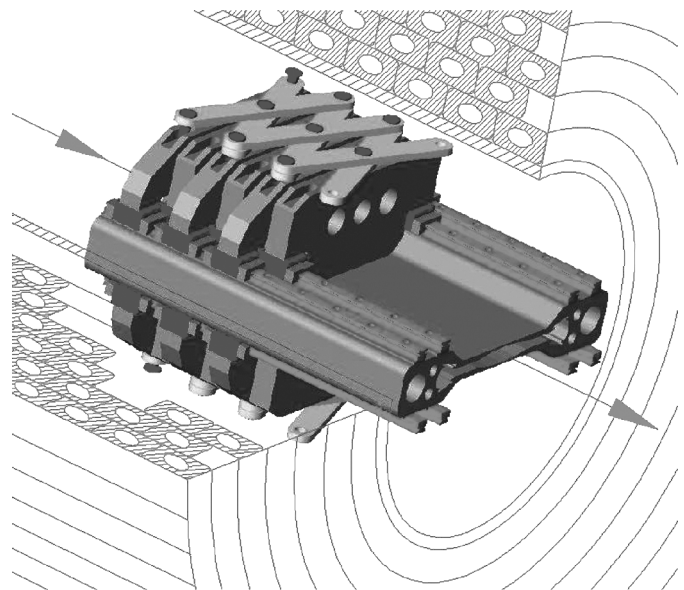
Figure 17
A three-dimensional schematic of the driving mechanism for a variable-period undulator placed outside a straight-section vacuum chamber. A section of the magnetic solenoid is also shown.

$$y' = P_y/p, \quad P_y' = (P_x - eA/c) \, e/(pc) \, \partial A/\partial y,$$
$$x' = (P_x - eA/c)/p, \quad P_x' = 0, \qquad (7)$$

where $'$ denotes differentiation over z. For a 'flat' undulator solenoid ($B_x = 0$) with length L, if $A = 0$ at the entrance ($z = -L/2$) and at the exit ($z = L/2$), the transport matrix may be written as

$$\begin{pmatrix} 1 & R_{12} & R_{13} & R_{14} \\ 0 & 1 & 0 & 0 \\ 0 & R_{32} & R_{33} & R_{34} \\ 0 & R_{42} & R_{43} & R_{44} \end{pmatrix}, \qquad (8)$$

and the symplecticity condition gives $R_{33}R_{44} - R_{43}R_{34} = 1$, $R_{13} = R_{32}R_{43} - R_{42}R_{33}$ and $R_{14} = R_{32}R_{44} - R_{42}R_{34}$. Then we can see that $R_{32} = 0$ and $R_{42} = 0$ are the conditions for decoupling. These matrix elements describe the dependence of y and y' on $x_0' = P_x/p$ at the entrance and the exit. To calculate this dependence, (7) may be rewritten as

$$y'' + 0.5\, \partial [eA(y,z)/(pc)]^2/\partial y = x_0'[e/(pc)]\, \partial A(y,z)/\partial y. \qquad (9)$$

The value of $eA/(pc)$ is small if the electron energy is high, and in the linear approximation in $eA/(pc)$ the matrix elements can be expressed as

$$R_{42} \simeq -e/(pc) \int_{-L/2}^{L/2} B_z(0,z)\, \mathrm{d}z,$$
$$R_{32} \simeq -e/(pc) \int_{-L/2}^{L/2} \int_{-L/2}^{z} B_z(0,z_1)\, \mathrm{d}z_1 \mathrm{d}z, \qquad (10)$$

where $B_z = -\partial A(y,z)/\partial y$. Thus, in this approximation, to make the coupling zero, both the first and the second integrals of the longitudinal field should be zero. The first integral reduces to zero when the total number of ampere-turns in the undulator and the compensating solenoids is zero. One way to reduce the second integral to zero is to make B_z an even function of z. The simplest example is a configuration with two identical guard solenoids, one at each end of the undulator solenoid, the total ampere-turns in the guard solenoids being equal to the total current in the undulator solenoid with the opposite sign.

Note that the above consideration is applicable for the 'two-dimensional' magnetic field

$$\mathbf{B}(y,z), \qquad B_x = 0. \qquad (11)$$

In particular, (11) describes a 'flat' undulator solenoid with a current directed along the x axis only. For solenoids with round coils, we can use iron insertions with horizontal slits to satisfy (11). These insertions produce an additional skew-quadrupole field. These considerations are also applicable to guard solenoids.

References

Billen, J. H. & Young, L. M. (2001). *LAACG Software – Poisson/Superfish*, http://laacg1.lanl.gov/laacg/services/possup.html.

Brown, G., Halbach, K., Harris, J. & Winick, H. (1983). *Nucl. Instrum. Methods Phys. Res.* **208**, 65–77.

Chae, Y. C. & Decker, G. (1996). *Proceedings of the 1995 Particle Accelerator Conference*, pp. 3409–3411. Piscataway, NJ: IEEE.

Chavanne, J., Elleaume, P. & Van Vaerenberg, P. (1998). *J. Synchrotron Rad.* **5**, 196–201.

Clarke, J. A. & Scott, D. J. (2001). *Proceedings of the 25th ICFA Advanced Beam Dynamics Workshop: Shanghai Symposium on Intermediate Energy Light Sources*, edited by J. Corbett, Z. M. Dai, D. Einfeld & Z. T. Zhao, Shanghai, China, 24–26 September 2001.

Dejus, R. J. & Sanchez del Rio, M. (1996). *Rev. Sci. Instrum.* **67**. CD-ROM.

Dejus, R. J., Vasserman, I. B., Sasaki, S. & Moog, E. R. (2002). Technical Bulletin ANL/APS/TB-45. Advanced Photon Source, Argonne National Laboratory, Argonne, IL, USA.

Den Hartog, P. K., Grimmer, J., Trakhtenberg, E., Wiemerslage, G. & Xu, S. (1997). *Proceedings of the 1997 Particle Accelerator Conference*, pp. 3556–3558. Piscataway, NJ: IEEE.

Geisler, A., Hobl, A., Schillo, M. & Rossmanith, R. (2001). *Proceedings of the Particle Accelerator Conference*, pp. 233–235. Piscataway, NJ: IEEE.

Gippner, P. (2001). *Status and Properties of the Hybrid Undulator U27*, http://www.fz-rossendorf.de/ELBE/en/fel/gippner2.html.

Gluskin, E. (1998). *J. Synchrotron Rad.* **5**, 189–195.

Halbach, K. (1981). *Nucl. Instrum. Methods Phys. Res.* **187**, 109–117.

Hara, T., Tanaka, T., Tanabe, T., Marechal, X. M., Okada, S. & Kitamura, H. (1998) *J. Synchrotron Rad* **5**, 403–405.

Ho, A. H., Pentell, R. H., Feinstein, J. & Haung, Y. C. (1991). *IEEE J. Quantum Electron.* **27**, 2650–2655.

Huang, Y. C., Wang, H. C., Pentell, R. H., Feinstein, J. & Harris, J. (1994). *Nucl. Instrum. Methods Phys. Res. A*, **341**, 431–435.

Huang, Y. C., Wang, H. C., Pentell, R. H., Feinstein, J. & Lewellen, J. W. (1994). *IEEE J. Quantum Electron.* **30**, 1289–1294.

Kitamura, H. (1998). *J. Synchrotron Rad.* **5**, 184–188.

Kornyukhin, G. A., Kulipanov, G. N., Litvinenko, V. N., Vinokurov, N. A. & Vobly, P. D. (1983). *Nucl. Instrum. Methods Phys. Res.* **208**, 281–284.

Lewellen, J. W., Schmerge, J. F., Haung, Y. C., Feinstein, J. R. & Pentell, H. (1995). *Nucl. Instrum. Methods Phys. Res. A*, **358**, 24–26.

Lewellen, J. W., Vinokurov, N. A., Shu, D. & Shenoy, G. K. (2003). In preparation.

Masuda, K., Kitagaki, J., Dong, Z.-W., Kii, T., Yamazaki, T. & Yoshikawa, K. (2001). *Nucl. Instrum. Methods Phys Res. A*, **475**, 608–612.

Rakowsky, G., Lynch, D., Blum, E. B. & Krinsky, S. (2001). *Proceedings of the Particle Accelerator Conference*, pp. 2453–2455. Piscataway, NJ: IEEE.

Sanchez del Rio, M. & Dejus, R. J. (1997). *Proc. SPIE*, **3152**, 148–157.

Shastri, S. D., Dejus, R. J. & Haeffner, D. R. (1998). *J. Synchrotron Rad.* **5**, 67–71.

Shenoy, G. K., Lewellen, J. W., Shu, D. & Vinokurov, N. A. (2002). Patent application in progress.

Shu, D., Lewellen, J. W. & Shenoy, G. K. (2003). In preparation.

Stefan, P., Krinsky, S., Rakowsky, G., Solomon, L., Lynch, D., Tanabe, T. & Kitamura, H. (1998). *Nucl. Instrum. Methods Phys. Res. A*, **412**, 161–173.

Tanabe, T., Marechal, X., Tanaka, T., Kitamura, H., Stefan, P., Krinsky, S., Rakowsky, G. & Solomon, L. (1998). *Rev. Sci. Instrum.* **69**, 18–24.

Varfolomeev, A. A., Ivanchenkov, S. N., Khlebnikov, A. S., Pellegrini, C., Baranov, G. A. & Michailov, V. I. (1992). *Nucl. Instrum. Methods Phys. Res. A*, **318**, 813–817.

Walker, R. P. (1993). *Nucl. Instrum. Methods Phys. Res. A*, **335**, 328–337.

Wulff, M. (2002). Private communication.

213